Lewis Base Passivation Mediates Charge Transfer at Perovskite Heterojunctions

Robert J. E. Westbrook[1,2,3], Thomas J. Macdonald[1,3] Weidong Xu[1,3], Luis Lanzetta[1,3], Jose M. Marin-Beloqui,[2] Tracey M. Clarke[2], Saif A. Haque[1,3]*

[1]Department of Chemistry, Imperial College London, Molecular Sciences Research Hub White City Campus, Wood Lane, W12 0BZ, UK

[2]Department of Chemistry, University College London, 20 Gordon Street, London WC1H 0AJ, UK

[3]Centre for Processable Electronics, Imperial College London, London SW7 2AZ, UK

*Corresponding author: S.A.H (s.a.haque@imperial.ac.uk)

Abstract

Understanding interfacial charge transfer processes such as trap-mediated recombination and injection into charge transport layers (CTLs) is crucial for the improvement of perovskite solar cells. Herein, we reveal that the chemical binding of charge transport layers to $CH_3NH_3PbI_3$ defect sites is an integral part of the interfacial charge injection mechanism in both n-i-p and p-i-n architectures. Specifically, we use a mixture of optical and X-Ray photoelectron spectroscopy to show that binding interactions occur via Lewis base interactions between electron donating moieties on hole transport layers and the $CH_3NH_3PbI_3$ surface. We then correlate the extent of binding with an improvement in the yield and longer lifetime of injected holes with transient absorption spectroscopy. Our results show that passivation-mediated charge transfer has been occurring undetected in some of the most common perovskite configurations and elucidate a key design rule for the chemical structure of next-generation CTLs.

TOC

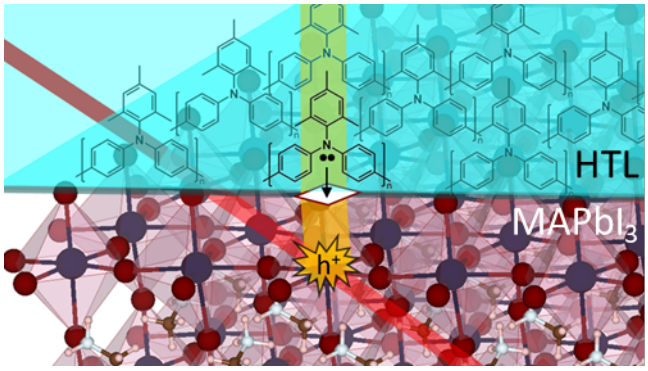

1. Introduction

Over the last decade, hybrid organic-inorganic perovskite solar cells (PSCs) have set themselves apart from other photovoltaic technologies with efficiencies over 25%,[1] rivalling the best inorganic materials. At the same time, their low-cost solution process lends them an energy payback time more similar to organic photovoltaics.[2] This extraordinary class of materials have the chemical formula, ABX_3 where A [= Cs, methylammonium, formamidinium] and B (= Pb, Sn) are cations and X (=I, Br) is an anion. PSCs usually consist of this layer – most commonly in its $CH_3NH_3PbI_3$ ($MAPbI_3$) form – sandwiched between two charge transport layers (CTLs) that aid the separation of electrons and holes towards the external circuit.

Many of the short comings of PSCs can be traced back to structural defects. Remarkably, harmful defects that form electronic states within the band-gap – i.e., traps - are found at relatively low concentrations in hybrid perovskites compared to other solution processed technologies,[3] but the termination of crystal symmetry at the surface and grain boundaries inevitably leads to a significant population at the interfaces with the CTLs.[4–6] Such defects limit the open-circuit voltage (V_{OC}) in $MAPbI_3$ to below the theoretical maximum of 1.33 V, ultimately limiting device power conversion efficiency (PCE).[7] Moreover, it is well known

that perovskites are rapidly degraded in the presence of oxygen and light.[8–11] We demonstrated that this happens because O_2 reacts with photoexcited electrons after adsorbing at iodide vacancies, forming highly aggressive superoxide (O_2^-) species.[12] Consequently, defect management has come to the fore as an effective solution to improve both the stability and overall device PCE of PSCs.[13]

In 2014, Noel *et al* showed that Lewis bases such as thiophene and pyridine could be used to coordinate to unsaturated Pb^{2+} ions (i.e. iodide vacancies) at the surface and grain boundaries of $MAPbI_3$.[14] The resulting dative bond between the electron donating moiety on the Lewis base and Pb^{2+} ions balances the positive charge that would otherwise trap electrons. Since then, this principle, known as passivation, has been expanded to include other small molecules and inert polymers.[15–19] This active sub-field has also successfully developed passivation strategies for negatively charged defects such as undercoordinated I^-, PbI_3^- antisites and A cation vacancies with myriad molecules including caffeine.[13,20]

CTL selection has been another important strand of perovskite research after Kim *et al* introduced the first solid-state PSCs in 2012.[21] Subsequently, research in this area has revealed a number of desirable properties for CTLs including energetic alignment to the perovskite layer, charge mobility and the addition of dopants.[22–24] Moreover, a small number of groups have reported passivation from charge transport layers including fullerenes,[25,26] n-type[27] and p-type molecules.[28,29] While these studies have demonstrated that passivation from CTLs can mitigate non-radiative recombination, ion migration and chemical instability in the perovskite layer, no one has yet addressed the impact that such interactions have on charge injection at the interfaces.

An outcome of Marcus theory is that the rate of electron transfer is partly determined by the nature of the intervening medium between donor and acceptor. In other words, the rate of transfer through bonds far exceeds that through space. We therefore posit that interactions between CTLs and the perovskite surface should enhance interfacial charge injection. While correlation between bonding strength and charge transfer was shown in 2001 to occur in Lewis acid-base complexes,[30] few studies have broached this subject in the field of perovskite or related solar cells. Seok and co-workers highlighted the important role of coordination interactions between the HTL and Sb_2S_3 in quantum dots.[31] Additionally, Bi *et al* suggested that the decreased coupling between $MAPbI_3$ and *spiro*-OMeTAD on account of its twisted *spiro* centre results in longer recombination lifetimes at the $MAPbI_3$/HTL interface relative to HTLs that form a 'face-on' configuration.[32] More recently, Jung *et al* achieved a remarkable PCE of 22% in P3HT-based n-i-p solar cells after functionalisation of $(FAPbI_3)_{0.95}(MAPbI_3)_{0.05}$ (FA = Formamidinium) with n-hexyl trimethyl ammonium bromide (HTAB).[33] They attributed this improvement in part to the improved contact between perovskite/P3HT due to alkyl-alkyl Van der Waal interactions, which enhance hole injection. Despite the excellent insight from these studies, conclusions tend to be drawn from macroscopic device performance and a limited range of materials, which cannot directly and universally link absorber/CTL interactions with charge injection yield.

Therefore, in this study we use a combination of transient absorption spectroscopy (TAS) and photoluminescence (PL) spectroscopy as an interface specific probe to show that binding interactions at $MAPbI_3$/CTL junctions mediate the charge injection process in both the n-i-p and p-i-n configurations for six $MAPbI_3$/CTL combinations. We demonstrate that such effects - while negligible at the high fluences usually associated with TAS – are critical at the relatively low fluences relevant to operational conditions of 1 Sun. This partially

explains the success of commercial CTLs such as PTAA and fullerene derivatives in contemporary PSCs and sets a precedent for the design of next-generation CTLs.

2. Results and Discussion

2. 1 Passivation-Mediated Charge Transfer in the n-i-p Architecture

2. 1. 1. Design of n-i-p Films

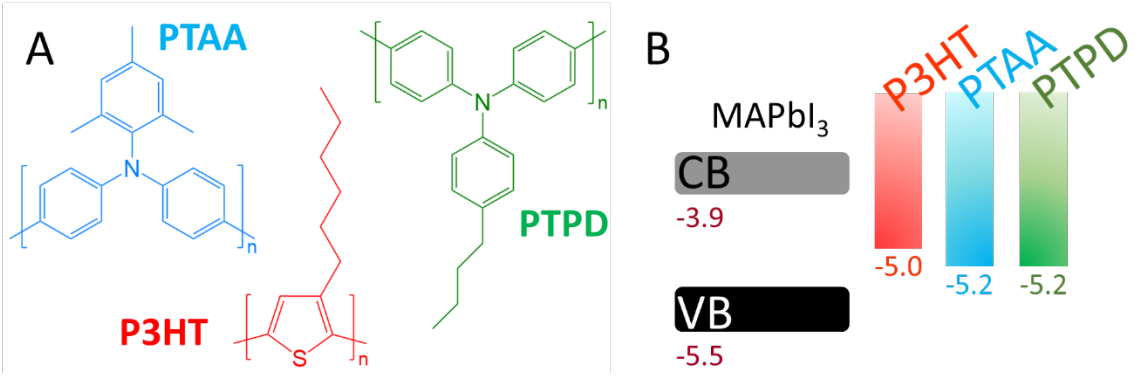

Fig. 1: (a) Chemical structures of PTAA, PTPD and P3HT hole transport layers. (b) Corresponding energetics at the $MAPbI_3$/HTL interface. Values in eV shown for $MAPbI_3$, PTAA, PTPD and P3HT are a three-paper average from photoelectron spectroscopy measurements in the literature, details in Table S1.

We interfaced $MAPbI_3$ with three well-known polymeric hole transport layers (HTLs): poly[bis(4-phenyl)(2,4,6-trimethylphenyl)amine] (PTAA), poly[N,N'-bis(4-butylphenyl)-N,N'-bisphenylbenzidine] (PTPD) and poly(3-hexylthiophene) (P3HT). The corresponding structures in Fig. 1a show that all three HTLs contain Lewis base passivating moieties, with PTAA and PTPD containing tertiary amine groups and P3HT containing a thiophene group. These functional groups have been shown to passivate iodide vacancies in $MAPbI_3$,[14] which in turn are known to provide sites for non-radiative recombination and superoxide formation.[12,34] When interfaced with $MAPbI_3$, all three HTLs are expected to drive efficient hole injection on account of the favourable interfacial energy offset in all cases, as shown in Fig. 1b.[22] The values for the HOMO and band energies of the HTLs and $MAPbI_3$ were obtained from separate photoelectron spectroscopy studies in the literature (details in Table S1), where the different materials were investigated in isolation. We note that

contacting the individual layers will alter the absolute values of the HOMO and band energies of $MAPbI_3$ and HTL to a degree. However, the *in-situ* energetic alignment in the specific case of $MAPbI_3$/HTL (HTL = PTAA, PTPD and P3HT) has been measured by Stolterfoht *et al*, who report a similar picture to that shown in Fig. 1b with PTAA and PTPD being better aligned to $MAPbI_3$ than P3HT.[35]

Samples were prepared via a one-step deposition of $MAPbI_3$ as reported elsewhere,[36] and HTLs were spin-coated on top of $MAPbI_3$ in order to form a 30 nm ± 3 nm thick layer (Fig S1, Table S2). Further details of sample processing can be found in the Experimental section. We also note that PTAA, PTPD and P3HT have similar wetting properties and thus we discard the role of surface energy variations in our below results.[37]

2. 1. 2 Passivation from Hole Transport Layers in n-i-p Films

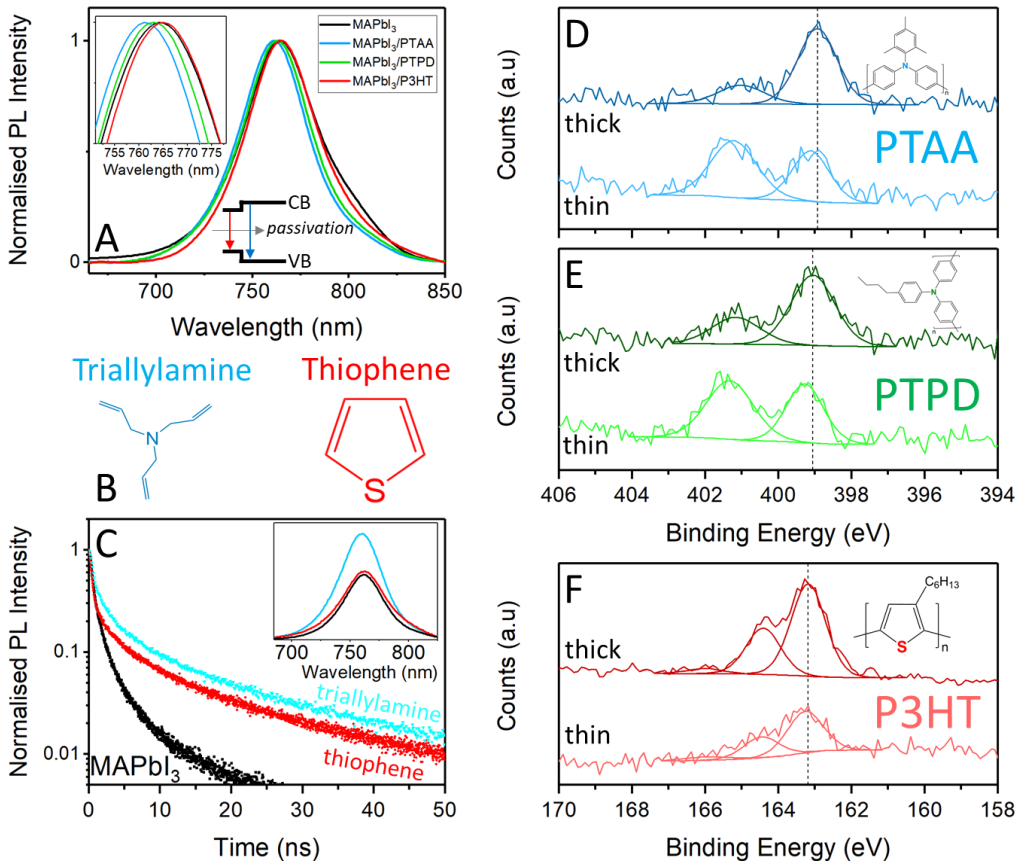

Fig. 2: Evidence for passivation. (a) normalised steady-state photoluminescence spectra for $MAPbI_3$ and $MAPbI_3$/HTL (HTL = PTAA, PTPD, P3HT) films. Insets: (top left) A close-up view of the peak maxima; (bottom) schematic illustrating the blue-shift of the photoluminescence peak after passivation. Films were excited at 510 nm. The passivating moieties on the HTLs were simulated by their "pseudomonomers": thiophene for P3HT and triallylamine for both PTAA and PTPD, structures in (b). (c) Radiative lifetime of $MAPbI_3$, $MAPbI_3$/thiophene and $MAPbI_3$/triallylamine excited at 635 nm (fluence: 0.11 nJ cm^{-2}); (inset) steady-state emission of the same samples excited at 510 nm. N 1*s* core level spectra for (d) $MAPbI_3$/PTAA and (e) $MAPbI_3$/PTPD films. (f) S 2*p* core level spectra for $MAPbI_3$/P3HT films. In each panel (d-f), the upper and lower spectra correspond to thick (30 nm) and thin (< 10 nm) HTL films. Structures of the HTLs (target element highlighted) are given in the insets.

To confirm passivation of $MAPbI_3$ by the HTLs, we looked to photoluminescence (PL) spectroscopy. Fig. 2a shows the PL spectra of $MAPbI_3$ and $MAPbI_3$/HTL (HTL = PTAA, PTPD, P3HT) samples (Raw spectra in Fig S2). In the case of $MAPbI_3$, peak emission was observed at $\lambda_{peak} = 764$ nm due to radiative recombination of electrons and holes across the 1.6 eV band gap. In the case where $MAPbI_3$ was interfaced with PTAA or PTPD, a blue-shift was observed. Such blue-shift in the $MAPbI_3$ emission has been attributed to passivation of emissive trap-states at the band edges.[26] The rationale for this is that in highly trapped films,

emission occurs on average from states closer together in energy due to the occupancy of trap states (Fig. 2a, red arrow). However, if passivation occurs, those trap-states cannot be filled, and emission takes place between states that are on average further apart in energy. The result is a blue-shift in the PL spectra (Fig. 2a, blue arrow). We found no change when P3HT was deposited on $MAPbI_3$, suggesting minimal passivation of band-edge trap-states in this case. This gives some indication that the passivation from the triarylamine HTLs is stronger than with P3HT.

To further confirm this, we also measured the steady-state PL spectra after excitation at 450 nm via the bottom ('substrate') and top ('film') sides respectively, results in Fig S3. Given the small penetration depth (< 15 nm) of this wavelength of light in the $MAPbI_3$ film, such measurements allow for observation of local changes in recombination behaviour. We find that in the case of $MAPbI_3$, the 'substrate' and 'film' PL spectra are perfectly overlaid, suggesting that the trap-state density at either location is similar. This behaviour is mirrored in the case of $MAPbI_3$/P3HT, suggesting the P3HT layer has little impact on the trap-state density. On the other hand, in the case of $MAPbI_3$/PTAA and $MAPbI_3$/PTPD, the 'film' PL is significantly blue shifted compared to the 'substrate', indicating that some passivation is occurring at the $MAPbI_3$/HTL interface.

Encouraged by this finding, we decided to isolate the passivation effect from the electron-donating moieties present on the HTLs by treating $MAPbI_3$ with their "pseudo-monomers". We selected triallylamine to simulate the tertiary amine groups on both PTAA and PTPD, and thiophene to simulate the thiophene group on P3HT. Their structures are indicated in Fig. 2b. We note that the ideal choice for the pseudo-monomer of the poly(triarylamines) would be a small-molecule arylamine such as triarylamine or one of its derivatives.

However, such small molecules are routinely used as hole conductors (Ionisation potential ~ 5.5 eV) in hybrid photovoltaics and as such it would be impossible to decouple passivation from injection.[38] Therefore, we used triallylamine (ionisation potential ~ 7.6 eV)[39] to ensure that hole injection could be ruled out of any change in PL intensity.

Steady-state PL (Fig. 2c inset) shows that triallylamine passivation increases the integrated PL intensity by 65%, while thiophene passivation has a more incremental effect (+16%). Interestingly, triallylamine passivation also results in a significant blue-shift of the $MAPbI_3$ emission, in agreement with that obtained for PTAA and PTPD in Fig. 2a. These findings are backed up by time-resolved PL (TRPL) studies measured at low excitation fluence (0.11 nJ cm^{-2}), presented in Fig. 2c. Unpassivated $MAPbI_3$ exhibits a rapid PL decay typical of charge trapping at the surface and grain boundaries as found elsewhere.[22,40] Addition of both triallylamine and thiophene leads to the formation of a second, longer-lived decay component associated with trap-mediated recombination in the bulk of the perovskite film. The appearance of this feature after treatment with the "pseudomonomers" is indicative of passivation of the perovskite surface. Moreover, this longer-lived component is more pronounced after triallylamine rather than thiophene treatment, suggesting the extent of passivation is greater in the former case.

Both the steady-state and time-resolved PL studies of $MAPbI_3$ treated with the pseudo-monomers provide strong evidence for the superiority of tertiary amine, relative to thiophene, functional groups in passivating iodide vacancies. This is in line with Noel *et al*, who also found that basic nitrogen groups – in their case from pyridine - are more capable than thiophene groups at passivating the $MAPbI_3$ surface.[14] Moreover, we also measured the PL dynamics of $MAPbI_3$ films treated with 3-hexylthiophene (3HT), the exact monomer

of P3HT, with details in Fig S4. In this case, we observe no enhancement in the PL decay lifetime, suggesting that trap-state passivation is minimal. We suggest that while pure thiophene is capable of passivating the $MAPbI_3$ surface, albeit less than triallylamine, 3HT is incapable of doing so, potentially due to steric hindrance associated with the bulky hexylthiophene chain. A similar mechanism was put forward by Noel *et al* to explain the lack of passivation in the case of *tert*-butylpyridine, even when pure pyridine was highly effective.[14]

Table 1: Parameters from XPS spectra. Recorded binding energies (E_b) are for N 1*s* (PTAA and PTPD) and S 2$p_{3/2}$ (P3HT). ΔE_b is the difference between E_b measured for the 30 nm and <10 nm films.

Sample	HTL thickness (nm)	E_b (eV)	ΔE_b (eV)
$MAPbI_3$/PTAA	30	398.90 ± 0.05	**0.2 ± 0.1**
	< 10	399.10 ± 0.05	
$MAPbI_3$/PTPD	30	399.05 ± 0.05	**0.2 ± 0.1**
	< 10	399.25 ± 0.05	
$MAPbI_3$/P3HT	30	163.20 ± 0.05	**0.0 ± 0.1**
	< 10	163.20 ± 0.05	

We further probed the extent of passivation with X-ray photoelectron spectroscopy (XPS). Fig S5 shows the C 1*s* spectra for PTAA, PTPD and P3HT deposited on top of $MAPbI_3$. The spectra agree well with those in the literature for pure HTL films, suggesting that the HTL layer is well formed and free from contaminants or degradation products.[41–43]

Next, we investigated the core-level spectra of the N 1*s* (PTAA and PTPD) or S 2*p* (P3HT) orbitals, as these atomic positions within the polymers were suspected of being responsible for the passivating interactions observed in Fig. 2a. We therefore expected an increase in

binding energy, E_b of the passivating element upon moving from the HTL bulk to probing the HTL/$MAPbI_3$ interface. In order to measure this, we prepared $MAPbI_3$ films with 'thick' (30 nm) and 'thin' (<10 nm) HTL overlayers to probe the bulk and interface respectively, manipulating the strong surface sensitivity of XPS. The resulting core-level spectra are summarised in Fig. 2d-f.

The N 1*s* core-level spectra of $MAPbI_3$/PTAA in Fig. 2d show two important features. The high binding energy peak at 401.05 eV is assigned to N in $MAPbI_3$[44] and the low binding energy peak at 398.90 eV is assigned to N in PTAA.[42] We observe a similar spectrum for $MAPbI_3$/PTPD samples (Fig. 2e) with the N 1*s* ($MAPbI_3$) and N 1*s* (PTPD) peaks centred at 401.25 eV and 399.05 eV respectively. Interestingly, the N 1*s* peaks associated with PTAA and PTPD were found at higher binding energies (399.10 and 399.25 eV respectively) in the thinner samples i.e. when the $MAPbI_3$/HTL interface was targeted. This suggests an interaction between the N atoms of the triarylamine HTLs and the $MAPbI_3$ surface.

The S 2*p* core-level spectra for $MAPbI_3$/P3HT samples are given in Fig. 2f. The spectra are readily fitted to a $2p_{1/2}/2p_{3/2}$ doublet from the S-atoms in the thiophene unit, with the two components centred at 164.40 and 163.20 eV respectively.[45] We also observed a weaker contribution centred at 166.0 eV, which has been attributed previously to slight oxidation of the polymer surface.[45] For the purpose of measuring the relative binding energy of the thick and thin films, we monitored the change in the $2p_{3/2}$ peak. In contrast to the PTAA- and PTPD-capped $MAPbI_3$ films, no increase in binding energy was observed upon moving from the P3HT surface to the $MAPbI_3$/P3HT interface.

The interaction between the different HTLs and the $MAPbI_3$ surface is summarised in Table 1, which shows the change in binding energy, ΔE_b for the three HTLs as a function of

distance from the $MAPbI_3$ interface. PTAA and PTPD show evidence of strong interfacial interactions with a ΔE_b of 0.20 ± 0.1 eV in both cases. On the other hand, P3HT demonstrates a less significant interaction with $\Delta E_b = 0 \pm 0.1$ eV. We therefore assert that the weak passivation effect displayed by P3HT is due to the weaker interaction between its thiophene moiety and the $MAPbI_3$ surface. On the other hand, the more significant passivation effect from PTAA and PTPD is underpinned by the relatively strong interfacial interactions between the tertiary amine group and $MAPbI_3$.

2. 1. 3. Passivation-Mediated Hole Injection in the n-i-p Architecture

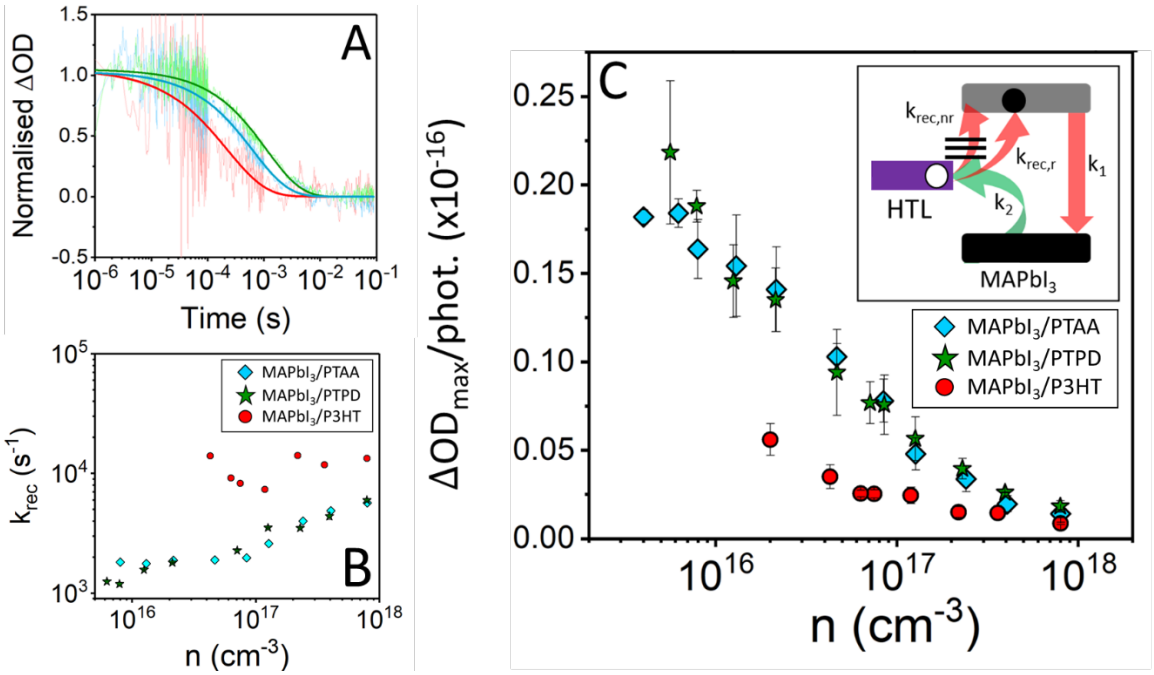

Fig. 3: Characterisation of hole injection in TiO_2/$MAPbI_3$/HTL (HTL = P3HT, PTAA, PTPD) films: (a) Normalised TA decays for the $MAPbI_3$/HTL films at $n \sim 2\text{x}10^{16}$ cm^{-3}. (b) Recombination rate constant, k_{rec} (taken as $1/\tau_{rec}$) over the same carrier-density range. (c) Relative hole injection yield, ΔOD_{max} normalised to photons absorbed, versus the initial carrier density, n in the $MAPbI_3$ layer. Inset: competing kinetic processes at the $MAPbI_3$/HTL interface. Samples were excited via the glass substrate at 510 nm and probed at the maximum of the HTL polaron absorption: 950 nm for P3HT and 1600 nm for PTAA/PTPD.

We next looked at how passivating interactions from HTLs at the $MAPbI_3$/HTL interface impact charge injection with intensity-dependent transient absorption spectroscopy (TAS). This technique allows one to track the development, transfer and relaxation of excited

states across femtosecond to millisecond timescales, provided those processes involve a change in the absorption characteristics of the film (ΔOD). Experimental details of our TAS set-up can be found in the supporting information and have been published elsewhere.[22]

Fig S6 displays the transient spectra of $MAPbI_3$/HTL films on Al_2O_3 (dashed line) and TiO_2 (solid line) as well as TiO_2/$MAPbI_3$ with no HTL (black lines). The TiO_2/$MAPbI_3$/HTL spectra contain broad features in the near infra-red in all cases, with the P3HT-capped samples exhibiting features at 950 nm and the PTAA- and PTPD-capped samples displaying a broad contribution centred beyond 1600 nm. Moreover, transient absorption from $MAPbI_3$ is zero on microsecond timescales (Fig S7). Given that direct excitation of the HTLs was avoided by exciting from the substrate at 510 nm (where TiO_2 does not absorb) and the $MAPbI_3$ layer absorbs 99.8% of the incident photons before they reach the HTL layer (Fig S8), the spectra can be assigned to the formation of hole polarons in the HTL (HTL^+) and/or electrons in TiO_2 (TiO_2^-) upon injection of the relevant charge carrier from the $MAPbI_3$ layer. However, we note that ΔOD in the case of TiO_2/$MAPbI_3$ (Fig S6, black lines) is zero at the TiO_2/$MAPbI_3$/P3HT maximum (950 nm), and an order of magnitude weaker than the TiO_2/$MAPbI_3$/PTAA and TiO_2/$MAPbI_3$/PTPD maxima (1600 nm). This is most likely due to the much smaller extinction coefficient of TiO_2 relative to the HTL polarons.[46] On the other hand, the TA features and absolute ΔOD of the $MAPbI_3$/HTL films on insulating Al_2O_3 – where electron injection is energetically forbidden - closely match those on TiO_2. We also note that the observed features closely match those of the chemically oxidised HTLs.[22,47] Consequently, we can assign the features at 950, 1600 and 1600 nm in the TiO_2/$MAPbI_3$/HTL (HTL = P3HT, PTAA, PTPD) spectra to the hole polarons of P3HT, PTAA and PTPD respectively, formed after injection of photoexcited holes from the $MAPbI_3$ layer.

Given the Beer-Lambert law, ΔOD is directly related to the concentration of injected holes in the HTL. Therefore, by tracking the initial intensity, ΔOD_{max} and subsequent decay of the polaron spectra, we can build up a picture of the hole injection yield and recombination kinetics respectively. In Fig S9 we show such decays for the example of a $MAPbI_3$/PTPD film over a range of excitation fluences. Each TAS decay can be modelled with a stretched exponential function: $\Delta OD \propto exp\left[-\left(\frac{t}{t_0}\right)^{\alpha}\right]$. This type of decay is consistent with recombination in systems that contain a significant amount of disorder.[48] Given the complex decay dynamics, we assign an approximate lifetime, τ_{rec} as the time taken for ΔOD to reach 50% of its original value.[48]

The better passivation performance of PTAA and PTPD versus P3HT is underlined by the kinetic traces shown in Fig. 3a. It is clear to see that recombination across the $MAPbI_3$/P3HT interface is faster than in the case of $MAPbI_3$/PTAA or $MAPbI_3$/PTPD. This provides further supporting evidence that PTAA and PTPD have a greater capacity to passivate defects at the $MAPbI_3$ surface thus increasing τ_{rec}.

We next sought to investigate how the recombination rate and injection yield change with the initial carrier density, n in the $MAPbI_3$ layer. The value of n can be extracted from the fluence under the assumption that each absorbed photon produces one electron/hole pair (details in Experimental Section). Therefore, by analysing TAS traces across this fluence range we were able to build up a picture of how τ_{rec} and ΔOD_{max} vary from 10^{15} to 10^{18} cm^{-3} (~1 to 1000 Suns).

Recombination processes at the $MAPbI_3$/HTL interface can be modelled by the following rate equation:

$$-\frac{dn_+}{dt} = k_{rec,nr}n_+ + k_{rec,r}n_+n + k_{rec,A}n_+n^2 \quad (1)$$

where n_+ is the initial density of injected holes on the HTL, n is the initial density of electrons in the perovskite layer, $k_{rec,nr}$, $k_{rec,r}$ and $k_{rec,A}$ are the 1st, 2nd and 3rd order recombination rate coefficients. However, in the specific case where all photoexcited electrons in the $MAPbI_3$ layer are trapped (i.e. n = 0), Equation 1 becomes:

$$-\frac{dn_+}{dt} = k_{rec,nr}n_+ \quad (2)$$

We can define an overall recombination rate, k_{rec}, as $1/\tau_{rec}$ – the lifetime extracted from the transient absorption decay. Crucially, in the limit of trap-mediated, monomolecular recombination at the $MAPbI_3$/HTL interface, k_{rec} will be independent of n, in line with Equation 2. On the other hand, if traps are well-passivated and there is a significant electron density, n, in the $MAPbI_3$ layer, recombination will also ensue via bimolecular recombination (and potentially Auger for $n > 10^{18}$ cm^{-3}) and k_{rec} will be dependent on n in line with Equation 1.

Examining our data in light of this, we observe in Fig. 3b that k_{rec} for injected holes in P3HT is independent of light intensity for the range covered, the hallmark of monomolecular (i.e. trap-mediated) recombination kinetics. On the contrary, the dependence of k_{rec} on n in the case of PTAA and PTPD shows that the recombination kinetics are of higher order above $n \sim 10^{17}$ cm^{-3}, a clear indicator of well-passivated traps. Therefore, this is evidence that the trap density at the $MAPbI_3$/P3HT interface is significantly higher than with PTAA- or PTPD-capped $MAPbI_3$.

From our analysis, we extract values of $k_{rec,nr}$ for PTAA-, PTPD- and P3HT-capped $MAPbI_3$ films at n = 4 x 10^{16} cm^{-3} as 2 x 10^3, 2 x 10^3, and 1 x 10^4 s^{-1} respectively. Therefore,

recombination in the P3HT-capped system is an order of magnitude faster than in the PTAA- or PTPD-capped system. These values are in good agreement with Stolterfoht *et al*, who noted an order of magnitude faster recombination current in P3HT- compared to PTAA- and PTPD-based films.[35] We have shown herein that this discrepancy can be attributed to the greater extent of interfacial trap passivation from PTAA and PTPD versus P3HT.

Next, we looked to understand how the different extents of passivation from PTAA, PTPD and P3HT on the perovskite affected the yield of hole transfer. Fig. 3c shows the relative hole yield, ΔOD_{max}, normalised for photons absorbed, as a function of n for the same TiO_2/$MAPbI_3$/HTL (HTL = PTAA, PTPD, P3HT) samples. The ΔOD_{max} shown is a three-sample average and the error bars indicate the standard deviation between the three repeats. The general shape of the individual curves presented therein can be explained in terms of the competing rates of recombination in the $MAPbI_3$ layer (k_1) and injection into the HTL (k_2) (Fig. 3c, inset).[40] At high carrier density ($n \geq 10^{18}$ cm^{-3}), recombination in $MAPbI_3$ is governed by fast, three-body Auger recombination where $k_1 > k_2$, resulting in low hole injection yields. As the carrier density is lowered (10^{16}-10^{18} cm^{-3}), recombination in $MAPbI_3$ becomes dominated by bimolecular recombination, which is slower, typically on the order of 10-100ns. In this case, $k_1 < k_2$ and so the hole injection yield increases. As we approach the low carrier-density limit of our TAS setup ($n \leq 10^{16}$ cm^{-3}), the recombination kinetics in the $MAPbI_3$ layer begin to be dictated by trap-mediated monomolecular recombination. Here, the hole injection yield starts to plateau. This range of behaviour has been observed previously for $MAPbI_3$/spiro-OMeTAD interfaces.[49]

However, the more intriguing aspect of Fig. 3c is the divergence between $MAPbI_3$/P3HT and $MAPbI_3$/(PTAA, PTPD) samples in the trap-limited regime. At high carrier-density when trap-

states are filled, the ΔOD_{max} of the HTLs is similar, as predicted by the favourable interfacial energetics given in Fig. 1b. However, ΔOD_{max} is three times higher for PTAA and PTPD relative to P3HT at $n \sim 10^{16}$ cm^{-3} when trap-states are not filled by photoexcited carriers and the effects of passivation become apparent. Additionally, the order of improvement goes P3HT < PTAA ~ PTPD, which agrees with the extent of passivation deduced from ΔE_b in Table 1.

We also measured ΔOD_{max} versus n for Al_2O_3/$MAPbI_3$/HTL films to rule out the contribution from TiO_2^- at 1600 nm as the reason for the enhanced hole injection yields in PTAA- and PTPD-capped films (Fig S10). In this system, the insulating character of Al_2O_3 means that hole injection to the HTL is the only energetically favourable means of interfacial charge injection. Therefore, given the striking resemblance between Fig S10 and Fig. 3c - with PTPD and PTAA exhibiting much greater hole injection yields than P3HT as the carrier density is lowered – we can confidently discard the impact of the TiO_2^- contribution.

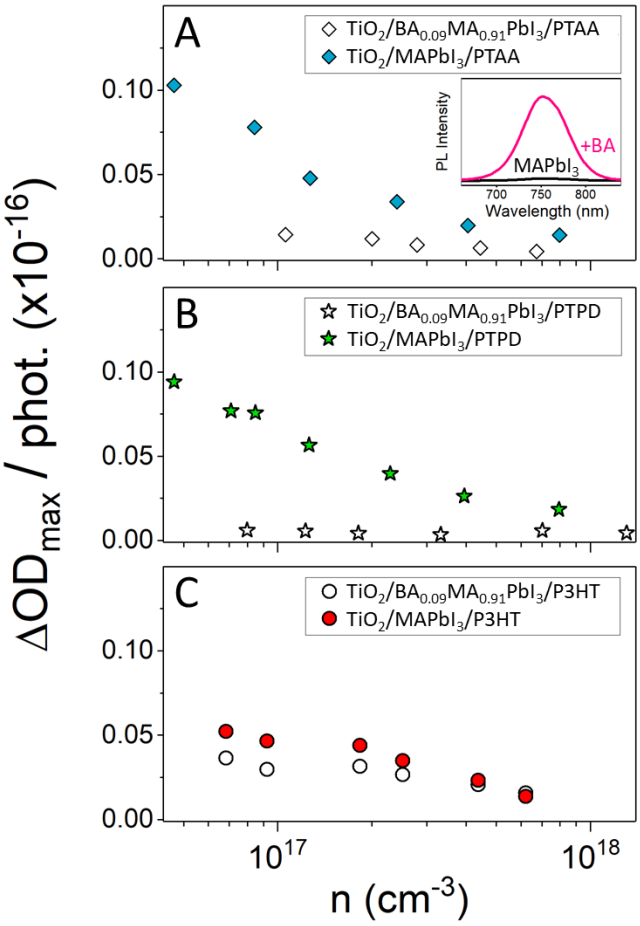

Fig. 4: Effect of perovskite trap density on hole injection. Relative hole injection yield, ΔOD_{max}, normalised per photon absorbed, as a function of the initial carrier density, n in the $MAPbI_3$ layer for $TiO_2/MAPbI_3$/HTL (coloured symbols) and $TiO_2/BA_{0.09}MA_{0.91}PbI_3$/HTL (white symbols), where HTL = (a) PTAA, (b) PTPD and (c) P3HT. Inset of (a): steady-state PL spectra of $MAPbI_3$ (black) and $BA_{0.09}MA_{0.91}PbI_3$ (magenta). Samples were excited via the glass substrate at 510 nm and probed at the maximum of the HTL polaron absorption: 950 nm for P3HT and 1600 nm for PTAA/PTPD.

We next designed an experiment to further probe passivation-mediated hole injection at the $MAPbI_3$/HTL interface by altering the extent to which the HTL could interact with defects at the $MAPbI_3$ surface. We measured the hole injection yield to the same HTLs in the case of both $MAPbI_3$ and its relatively trap-free $BA_{0.09}MA_{0.91}PbI_3$ (BA = butylammonium) counterpart. The lower trap-density of $BA_{0.09}MA_{0.91}PbI_3$ is demonstrated by the PL spectra in the inset of Fig. 4a, in which $BA_{0.09}MA_{0.91}PbI_3$ yields 39-times more intensity compared to $MAPbI_3$. This has previously been attributed to the passivation of $MAPbI_3$ grain boundaries by microscopic 2D domains.[50] Therefore, the highly passivated nature of the perovskite in

this case should limit the extent to which the HTLs can interact with defects at the surface. We also note that the valence band minimum remains unchanged for $BA_{0.09}MA_{0.91}PbI_3$.[50] Therefore, any changes in the hole injection yield are likely to be due to passivation alone.

Fig. 4a-c shows the relative hole injection yield, ΔOD_{max} for perovskite/HTL samples (perovskite = $MAPbI_3$, $BA_{0.09}MA_{0.91}PbI_3$; HTL = PTAA, PTPD, P3HT) as a function of n. For PTAA-capped films, the hole injection yield is significantly higher for $MAPbI_3$ than for $BA_{0.09}MA_{0.91}PbI_3$. Furthermore, a similar trend is observed for $MAPbI_3$/PTPD samples. This suggests that the lower defect density at the $BA_{0.09}MA_{0.91}PbI_3$ surface limits the injection yield by blocking binding interactions. We again see very little dependence on trap-state density in the case of P3HT regardless of the perovskite layer used, adding further weight to the argument that passivation does not play a significant role in the hole injection process for this HTL. Additionally, little distinction can be made between the effectiveness of the three HTLs on $BA_{0.09}MA_{0.91}PbI_3$, suggesting that it is the passivating interactions that allow PTAA and PTPD to outperform P3HT in $MAPbI_3$-based systems.

2. 1. 4. Passivation-Mediated Hole Injection in n-i-p Devices

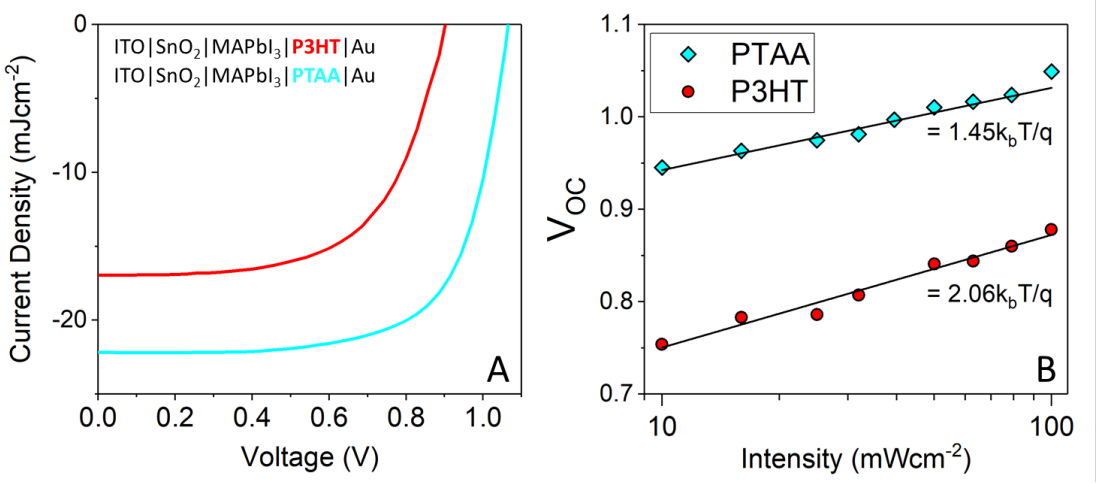

Fig. 5: Characterisation of ITO/SnO_2/$MAPbI_3$/HTL/Au (HTL = PTAA, P3HT) devices: (a) Current-voltage (J-V) characteristics; (b) intensity dependence of the open-circuit voltage (V_{OC}) and the relevant ideality factors.

Table 2. J-V parameters for the ITO/SnO_2/$MAPbI_3$/HTL/Au (HTL = P3HT, PTAA) devices displayed above.

HTL	J_{SC} (mAcm^{-2})	V_{OC} (V)	FF	PCE (%)
P3HT	17.10	0.902	0.612	9.45
PTAA	22.35	1.065	0.674	16.19

We measured the current-voltage (J-V) characteristics of ITO/SnO_2/$MAPbI_3$/HTL/Au (HTL = PTAA, P3HT) devices in order to understand the effect of passivation under working conditions. For this study, experimental control was valued over device PCE and so we avoided the use of additives, which complicate the picture of passivation and interfacial charge extraction. Therefore, in order to ensure the best comparison between thiophene- and triarylamine-based HTLs, we decided to omit PTPD from the following discussion on account of its order of magnitude lower mobility relative to PTAA in its undoped form.[51] We suggest that while PTPD is highly capable of extracting holes from $MAPbI_3$ – as evidenced by our TAS studies - the low hole mobility of this HTL could hinder the subsequent hole transport towards the gold contact. We therefore focus the following discussion on n-i-p devices that incorporate PTAA and P3HT, which are more prevalent in the literature.[33,52]

We attach a reference J-V curve in Fig S11 for an ITO/SnO_2/$MAPbI_3$/PTAA/Au device, where PTAA contained additives bis-(trifluoromethane) sulfonimide lithium salt (Li-TFSI) and 4-tert-Butylpyridine (tBp) to achieve high hole mobility and conductivity.[53] We achieve a PCE of 19.2% with this device, which is well in line with other reports in the literature on pure $MAPbI_3$-based n-i-p solar cells.[54]

The J-V characteristics for the undoped PTAA- and P3HT-based devices at 1 sun are presented in Fig. 5a, with the relevant device parameters listed in Table 2. The cells

incorporating PTAA were observed to perform markedly better than those using P3HT, with efficiencies of 16.19% and 9.45% respectively. This difference was driven by improvements in both the short-circuit current (J_{SC}; 17.10 to 22.35 mAcm^{-2}) and open-circuit voltage (V_{OC}; 0.902 V to 1.065 V). As evidenced by our TAS results in Fig. 3c, hole injection is much enhanced at $MAPbI_3$/PTAA interfaces relative to those involving P3HT. Therefore, we expect this, as well as the greater mobility of PTAA[51] to be factors in the improved J_{SC} in PTAA-based devices.

The V_{OC} is defined as the quasi-Fermi energy splitting of electrons and holes under illumination and is consequently intertwined with (i) the trap-state density and (ii) the energetic alignment at the perovskite/HTL interface. We have shown throughout this work that non-radiative recombination at the $MAPbI_3$/PTAA interface is significantly supressed relative to $MAPbI_3$/P3HT, most likely due to enhanced passivation from PTAA. To isolate the impact of passivation, we measured the V_{OC} as a function of light intensity. In the case of pure bimolecular recombination, the slope of the semi-logarithmic plot in Fig. 5b should be equal to the thermal voltage, k_bT/e.[55] However, in the presence of trap-mediated recombination the slope deviates towards steeper values, with a value of $2k_bT/e$ being the fingerprint of pure monomolecular recombination.[56] Intermediate situations with $n_{ID}.k_bT/e$ $(1 < n_{ID} < 2)$ can then be assessed by their ideality factor, n_{ID}.[57]

The device incorporating P3HT as the HTL demonstrates an n_{ID} of 2.06, indicating that recombination occurring in the device is dominated by monomolecular trap-mediated recombination. On the other hand, a marked improvement was observed when PTAA was used, with n_{ID} reduced to 1.45. We therefore conclude that PTAA reduces trap-mediated recombination in the $MAPbI_3$ layer to a greater extent than P3HT, contributing to the

enhanced V_{OC} in PTAA-based devices. We note that poor energetic alignment will also contribute to the lower V_{OC} of P3HT-based devices.[35]

2. 2. Passivation-Mediated Charge Injection in the p-i-n Architecture

2. 2. 1. Hole injection in the p-i-n Architecture

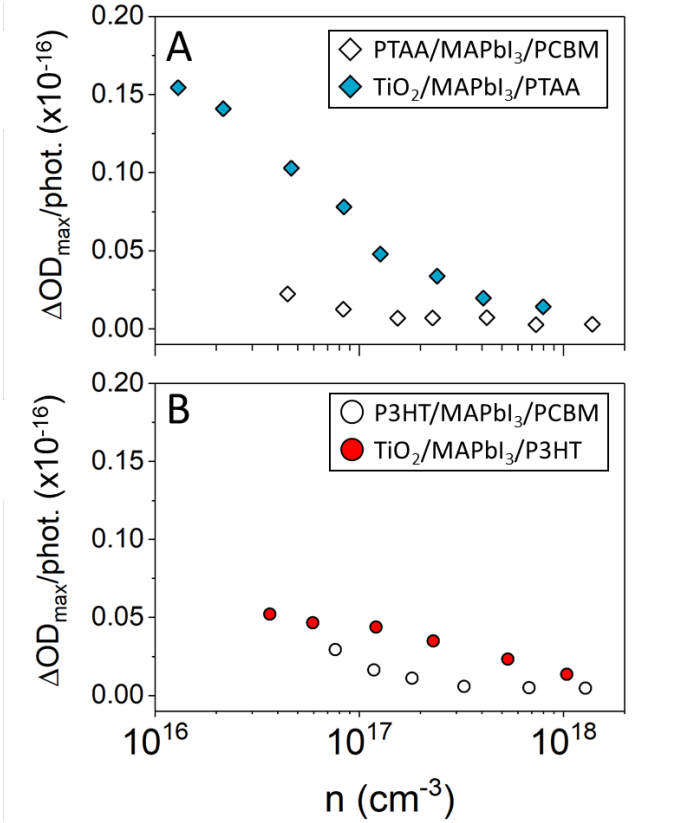

Fig. 6: Effect of architecture on hole injection. (a,b) Relative hole injection yield, ΔOD_{max}, normalised per photon absorbed, as a function of the initial carrier density, n, in the $MAPbI_3$ layer for n-i-p (TiO_2/$MAPbI_3$/HTL) and p-i-n (HTL/$MAPbI_3$/PCBM) films (HTL = PTAA and P3HT). Samples were excited at 510 nm via the glass substrate and probed at the maximum of the HTL polaron absorption: 950 nm for P3HT and 1600 nm for PTAA.

The p-i-n architecture is the most widely used in contemporary high-performance PSCs on account of the increased resistance towards hysteresis and UV-light.[58,59] Therefore, we also investigated the impact of passivation on interfacial charge injection in this class of materials. Firstly, we explored the impact on *hole* injection upon switching the HTL from top

layer to bottom layer. To do this, we prepared p-i-n (HTL/$MAPbI_3$/PCBM) and n-i-p (TiO_2/$MAPbI_3$/HTL) films and compared hole injection in the range, $10^{16} < n < 10^{18}$ cm^{-3}.

Fig. 6a and b show the relative hole injection yield, ΔOD_{max}, normalised per photon absorbed, as a function of n for $MAPbI_3$/PTAA and $MAPbI_3$/P3HT in the two architectures. For PTAA, a stark contrast between p-i-n and n-i-p configurations is observed, with the hole injection yield being four times higher in the latter case at n = 4 x 10^{16} cm^{-3}. Conversely, hole injection across the $MAPbI_3$/P3HT interface is similar irrespective of the architecture.

We have shown throughout this work that TAS can give unique insight into the chemical interactions at $MAPbI_3$/CTL interfaces. It is our view then, that the results in Fig. 6 can be rationalised in terms of the differing chemical interactions in the two architectures. Specifically, in the p-i-n architecture, a Poly [(9,9-bis(3'-(N,N-dimethylamino)propyl)-2,7-fluorene)-alt-2,7-(9,9–dioctylfluorene)] (PFN) interlayer must be placed between the HTL substrate and $MAPbI_3$ layer in order to improve the wetting of the latter.[60] This limits the extent of chemical interactions between the HTL and $MAPbI_3$ layers. Moreover, while there are some reports of passivation from underlayers,[61] it is possible that the change in architecture limits the scope of such interactions. Therefore, we expect passivation at the $MAPbI_3$/HTL interface in the p-i-n architecture to be obstructed. Conversely, in the n-i-p architecture, the HTL is deposited directly on top of the $MAPbI_3$ layer, allowing it to interact with the active layer surface.

We therefore postulate that the four-times lower hole injection yield upon switching from n-i-p to p-i-n architecture in the case of PTAA is due to the obstruction of passivation and the resulting decrease in interaction between the two layers. On the other hand, the similarity between p-i-n and n-i-p for P3HT-based films suggests that passivation-mediated

hole injection is negligible in either case. This provides further evidence that passivation plays a critical role in the high hole injection yields exhibited by some HTLs e.g. PTAA.

2. 2. 2 Passivation-Mediated Electron Transfer in the p-i-n Architecture

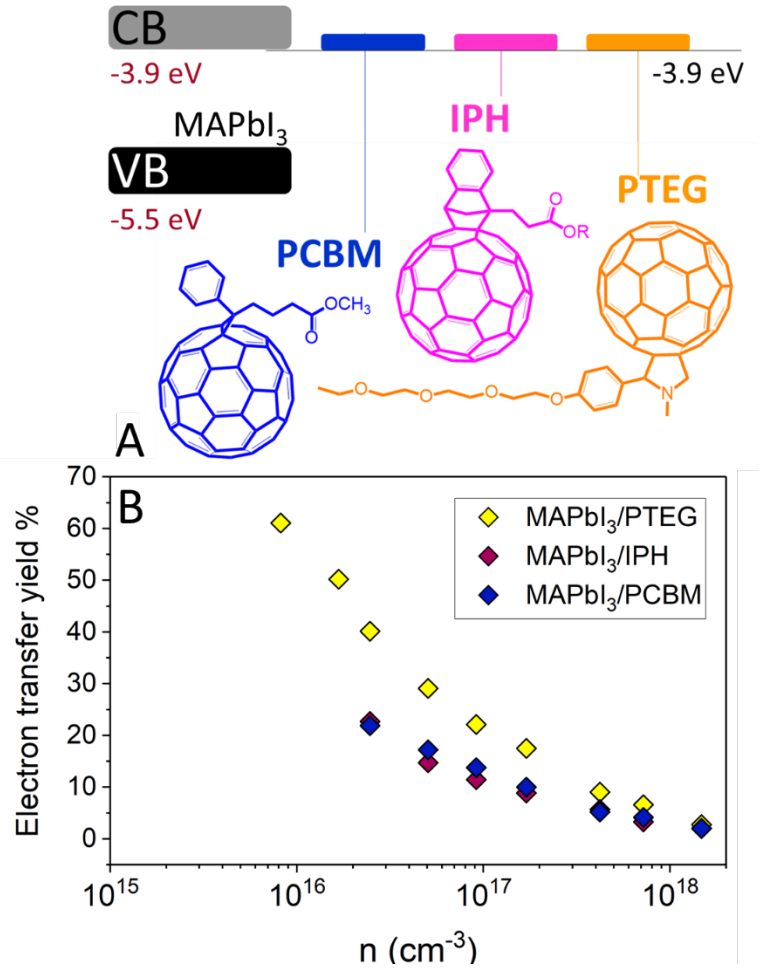

Fig. 7: a) Schematic illustrating the interfacial energetics at the $MAPbI_3$/ETL interface (ETL = PCBM, IPH and PTEG),[62] as well as the ETL structures. (b) Electron injection yield as calculated from transient absorption spectroscopy. Samples were excited via the glass substrate at 510 nm and probed at 925 nm, 1000 nm and 1000 nm for PTEG-, IPH- and PCBM-capped films.

We next investigated whether *electron* injection at the top interface in p-i-n films is affected by passivation. To do this, we interfaced $MAPbI_3$ with three fullerene-derivatives: [6,6]-phenyl-C61-butyric acid methyl ester (PCBM), indene-C60-propionic acid hexyl ester (IPH) and a fulleropyrrolidine with a triethylene glycol monoethyl ether side chain (PTEG). The structures given in Fig. 7a show that the ETLs contain functional groups capable of Lewis

base passivation. PCBM and IPH contain lone-pair oxygen in the form of C=O and C-O-C bonds, while PTEG has numerous possibilities including an oxygen-rich triethylene glycol chain and a tertiary amine group. Indeed, it has been shown that electron donating functionalities on such fullerene derivatives can bind to the perovskite at iodide vacancy (V_I) sites.[63,64] The extra passivating power of PTEG has been shown previously by Shao *et al* to be a factor in boosting the PCE of $MAPbI_{3-x}Cl_x$ cells to higher values than could be achieved with PCBM.[57] Moreover, all three ETLs have a similarly favourable LUMO energy relative to the $MAPbI_3$ conduction band (Fig. 7a).[62]

Here, we focus on how such passivation impacts electron injection with intensity-dependent TAS. Fig S12 gives the transient spectra of $MAPbI_3$/ETL (ETL = PCBM, IPH, PTEG) on hole conducting PTPD (circles) and insulating Al_2O_3 (triangles) taken 1 µs after excitation at 510 nm. In the PTPD/$MAPbI_3$/ETL samples we expected features from both PTPD and the ETL, whereas in the Al_2O_3/$MAPbI_3$/ETL samples we expected features purely from the ETL due to the insulating nature of Al_2O_3. Indeed, the samples deposited on PTPD show the characteristic absorption associated with hole polarons on the PTPD (peak at 1600nm) and another contribution centred around 1000 nm for PTPD/$MAPbI_3$/(PCBM, IPH) and 925 nm for PTPD/$MAPbI_3$/PTEG. Given that (i) the 900-1000 nm peaks do not feature in the $MAPbI_3$/PTPD spectrum (black squares), (ii) the 900-1000 nm peaks are clearly resolved in Al_2O_3/$MAPbI_3$/ETL films (triangles), and that (iii) the $MAPbI_3$ transient absorption is zero at 1µs (Fig S7); we assign the 900-1000 nm peaks to the ETL anion, formed after electron injection from $MAPbI_3$. This is in line with the transient spectrum of PCBM measured by Ohkita and Ito.[65]

Given this assignation, the raw change in optical density, ΔOD obtained from TAS measurements for the different $MAPbI_3$/ETL combinations can be used to estimate the electron injection yield, via the Beer-Lambert law:

$$Yield = \frac{n_-}{n} = \frac{\Delta OD_{max}.N_A}{1000.\varepsilon_-}\frac{1}{n} \quad (3)$$

where n_-, n, ε_- and N_A are the area density of fullerene anions in the ETL (cm^{-2}), area density of photoexcited electrons in the $MAPbI_3$ layer (cm^{-2}), extinction coefficient of the fullerene anion (6000 $M^{-1}\,cm^{-1}$)[65] and Avogadro's constant respectively. We obtain ΔOD_{max} as the value of ΔOD at 1 µs in the raw transient absorption spectra and n by assuming that every photon absorbed by the perovskite is converted to an electron/hole pair.

The electron injection yield as measured by TAS is outlined in Fig. 7b. In the high-irradiance limit, the performance of the ETLs is similar, as one would predict from their identical LUMO levels. However, as the intensity of excitation is decreased, we start to see significant distinctions between the different ETLs. Interestingly, PTEG outperforms the other fullerenes at 2 x 10^{16} cm^{-3}, while PCBM and IPH have almost identical responses as the intensity is lowered. In this experiment, we assumed that the contribution from the PTPD polaron at the ETL anion maximum was negligible. We note that any overlapping tail absorption from the PTPD polaron would only serve to over-estimate the IPH and PCBM electron yields relative to PTEG. Therefore, given that PTEG has a higher electron transfer yield than PCBM and IPH in spite of this, we are confident with our conclusion.

2. 3. Discussion

In this study, we investigated the intensity dependence of hole or electron injection from $MAPbI_3$ to the HTL or ETL top contact as a function of carrier density, n in the $MAPbI_3$ layer.

Importantly, significant divergence in the injection behaviour was found when moving from $n \sim 10^{18}$ cm^{-3} (~500 Suns) to $n \sim 10^{15}$ cm^{-3} (~ 1 Sun) – i.e., the domain of conventional solar cells. Specifically, those CTLs that were capable of passivating the top surface of the perovskite were able to produce greater charge transfer yields as the light intensity approached 1 Sun. In the following we outline the interfacial chemistry responsible for this effect, and discuss important implications for the design of perovskite optoelectronic devices.

We found that the passivation from the triarylamines PTAA and PTPD (TAAs), was far superior compared to thiophene-based P3HT. To explain these findings, it is interesting to qualitatively compare the Lewis basicity of the monomer units in the case of the TAAs and P3HT. Firstly, the hybridization of the passivating N atom in the TAAs is sp^3, compared to the sp^2 hybridization of the passivating S in P3HT, making electron donation more facile in the former. Additionally, nitrogen has a slightly larger electronegativity (3.0, Pauling scale) compared to that of sulfur (= 2.6). This, combined with the much stronger inductive effect from the three aryl groups, suggests that the electron density at the passivating N group in TAAs is greater than S in P3HT, giving the TAAs greater capacity to coordinate to the perovskite surface via Lewis base passivation. The same rationale was used by Zhao *et al* who showed that increasing the electron density at the passivating O group in R-X=O amino acids – by tuning X from electronegative sulfur (=2.58) to less electronegative phosphorous (=2.19) – could enhance the extent of Lewis base passivation and increase PCE from 20.46% to 22.35%.[17] Elsewhere, Wu *et al* showed that increasing the electron density at the passivating carboxylate group in donor-π-acceptor molecules, results in better binding to V_I sites on the perovskite and an increase in efficiency from 18.52% to 20.43%.[66] We discard

the idea that the greater electronegativity of N compared to S hinders electron donation, given that the electronegativity is still lower than that of oxygen, which is routinely used in Lewis bases for perovskite passivation, often in the form of C=O bonds.[15,17,66]

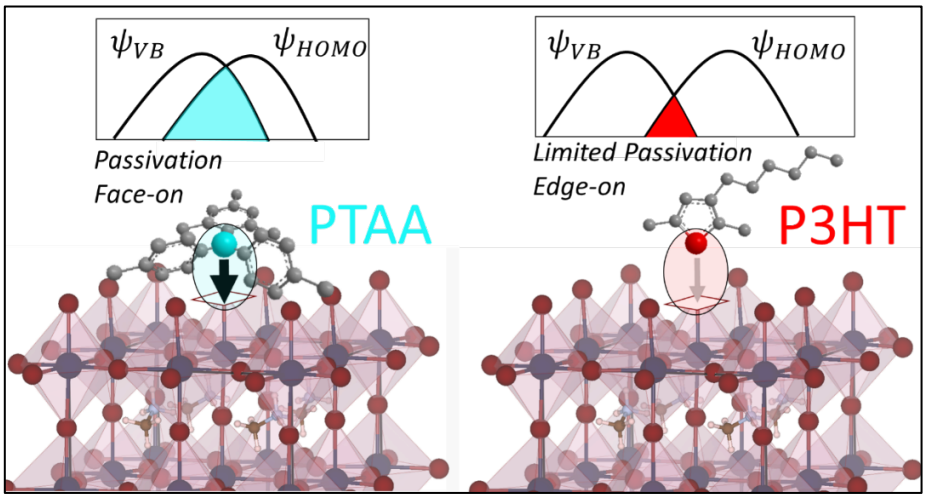

Fig. 8: Illustration of Passivation-Mediated Charge Transfer at the Perovskite/CTL Interface for PTAA and P3HT. Iodide vacancies (V_I) are indicated by the empty brown squares. **Left panel**: strong passivating interactions and a 'face-on' geometry lead to good overlap between the wavefunctions of the perovskite valence band, ψ_{VB} and the HTL HOMO, ψ_{HOMO}. **Right panel**: weaker passivating interactions and an 'edge-on' interaction geometry lead to poor overlap between ψ_{VB} and ψ_{HOMO}.

We subsequently found that such Lewis base passivation of V_I sites is correlated with the yield of interfacial charge injection. This could be partly explained by the lower non-radiative recombination rate, $k_{rec,nr}$ in the TAAs compared to the P3HT, but this does not account for the drop off in hole injection yield for the TAAs when $BA_{0.09}MA_{0.91}PbI_3$ – with it's lower trap density and thus lower $k_{rec,nr}$ - is used instead of $MAPbI_3$ (Fig. 4). To explain this, we put forward the idea of passivation-mediated charge transfer, summarized in Fig. 8. This can be understood in terms of the Marcus theory of electron transfer, by which increased overlap between donor and acceptor wavefunctions leads to enhanced rates of charge transfer. We propose that the strong passivating interactions between N atoms on the TAAs (Fig. 8, left panel; blue) and V_I (Fig. 8, brown squares) at the perovskite surface leads to enhanced coupling between the perovskite VB and HTL HOMO, thus increasing the hole

injection yield (Fig. 8, top left). In the case of P3HT, the lack of V_I passivation from S on P3HT (Fig. 8, right panel, red) results in limited coupling between the perovskite VB and P3HT HOMO (Fig. 8, top right), and thus lower hole injection yields.

Moreover, consideration of the interaction geometry in Fig. 8 reveals a second factor that could determine the extent of wavefunction overlap and ultimately interfacial injection. In order for the TAAs to interact with the perovskite surface at V_I sites, the monomer unit must interact with the perovskite surface in a 'face-on' configuration, ensuring close proximity between the perovskite surface and the conjugated backbone of the triarylamine. On the other hand, the optimum interaction geometry for P3HT would be 'edge-on', where the conjugated backbone of the polymer would lie out of plane with the perovskite surface. Therefore, the close proximity and in-plane nature of perovskite/TAA interface should work to enhance the cross section for interfacial charge injection.[67]

Chemical intuition suggests that close proximity between donor and acceptor at the perovskite/HTL interface should be a double-edged sword. As we have shown here, passivating interactions lead to large injection yields due to increased overlap between the perovskite VB and HTL HOMO. By the same token, it has been suggested elsewhere that such overlap increases interfacial recombination and reduces device performance for some perovskite/HTL combinations.[32,68] It is therefore curious that PTAA and PTPD offer the best of both worlds, in that they exhibit high injection yields and slow recombination lifetimes. We propose that this is because the strong passivating interactions in this case have the dual effect of increasing the overlap between the perovskite VB and the PTAA or PTPD HOMO, and mitigating charge trapping. In the case of P3HT, there is little evidence for passivation resulting in poorer extraction and a large amount of interfacial recombination.

This supports the hypothesis of Heo *et al*, who suggested that the higher PCE of $MAPbI_3$ devices based on triarylamine- rather than thiophene-based HTLs was due to the enhanced interfacial interaction in the former case.[69] Indeed, PSCs incorporating P3HT have recently surpassed 20% but not without extensive modification of the perovskite surface to enhance interfacial interactions.[33] This was achieved by functionalising the perovskite surface with n-hexyl trimethyl ammonium bromide (HTAB), which simultaneously passivates the perovskite and improves the P3HT/perovskite contact via alkyl-alkyl Van der Waal interactions, enhancing hole injection.

Consideration of the ETL structures results in an analogous conclusion around CTL passivation. It is established that PTEG has a greater capacity to passivate V_I vacancies compared to IPH and PCBM.[57] This has can be explained in terms of the passivating moieties on the individual ETLs. While the structures of IPH and PCBM are different, they contain the same amount of C=O and C-O-C groups capable of binding to V_I at the $MAPbI_3$ surface. On the other hand, PTEG has a much stronger propensity to passivate on account of its extra electron-donating functionalities in the form of ethylene glycol and tertiary amine groups. The resultant interactions with the $MAPbI_3$ surface result in enhanced wavefunction overlap, and thus electron injection, in a similar way to that observed with the HTLs. We expect this interaction to be at the heart of the 11.69% to 15.71% improvement of PSC device performance upon switching PCBM for PTEG observed elsewhere.[57]

All of this points to the critical nature of the perovskite/CTL interaction in determining efficiency of interfacial charge injection processes and ultimately of devices. Careful design of next-generation CTLs with passivating functionalities, or interfacial modifiers that enhance interactions with non-passivating CTLs, could improve interfacial charge injection,

supress non-radiative recombination and enhance stability. Furthermore, work is currently underway to understand and control strain-induced recombination in the perovskite layer.[70,71] However, the effect of strain exerted by CTLs on the perovskite remains unknown and should be the focus of future studies.

Finally, the impact of this study is not limited to PV applications: passivating CTLs could also boost the efficiency of perovskite light-emitting diodes (PeLEDs) according to the same principles. We note also that Lewis base passivation of B^{2+} (B = Pb, Sn) has been documented as an effective defect management strategy for PSCs based on ”triple-cation”,[72] MA-free[73] and Pb-free perovskites.[74] We therefore expect our findings on passivation-mediated injection to apply to these systems too.

3. Conclusions

In summary, we showed that passivation is an important part of the charge injection mechanism at the interfaces of PSCs. PL spectroscopy confirmed strong passivation in the case of PTAA- and PTPD- but not P3HT-capped films. By conducting PL studies on triallylamine and thiophene, we found the most likely mechanism was via Lewis base passivation from the tertiary amine groups on PTAA and PTPD with little effect from thiophene on P3HT. XPS further confirmed this as the binding energy of the N 1*s* orbital in PTPD and PTAA was significantly increased upon approach to the $MAPbI_3$/HTL interface, but no such effect was found with S 2*p* in P3HT. Crucially, TAS measurements showed that the yield and lifetime of injected charges were much enhanced in those HTLs that underwent strong binding interactions. This partially explains why PTAA outperforms P3HT as a HTL in PSCs. We also showed that this is the case for ETLs in the p-i-n architecture where PTEG outperformed PCBM and IPH on account of its numerous passivating moieties. The results

reported herein reveal a new aspect to the charge injection mechanisms in PSCs, which should be considered in the design of next-generation CTLs for perovskite optoelectronics.

4. Experimental Section

Materials

All materials were purchased and used as received. PbI_2 was purchased from Alpha Aesar. Mp-TiO_2 and methylammonium iodide (MAI) were purchased from Dyesol. Butylammonium iodide (BAI), mp-Al_2O_3, anhydrous dimethylsulfoxide (DMSO), anhydrous γ-butyrolactone (GBL), anhydrous chlorobenzene, methanol (MeOH), P3HT, triallylamine (TAA), 3-hexylthiophene (3HT) and thiophene (T) were purchased from Sigma Aldrich. PTAA, PTPD, PCBM and IPH were acquired from Ossila and PTEG from Solenne BV. PFN was bought from 1-material.

Film Fabrication

Glass slides were washed in deionised water, acetone and isopropanol (IPA) for 15 minutes followed by O_2 plasma treatment. Al_2O_3 substrates were prepared by making up a 6.67wt% solution of Al_2O_3 nanoparticles in IPA and spin-coating at 6000 rpm immediately after O_2 plasma treatment. TiO_2 substrates were prepared by making up a 2:7 (weight) solution of TiO_2 paste in EtOH, spin-coating on the glass immediately after plasma treatment, drying at 90 ^oC for 10 minutes and annealing at 450 ^oC for 45 minutes.

$MAPbI_3$ was deposited according to the method of Jeon *et al*.[36] PbI_2 and MAI were mixed together in a 1:1 ratio at a concentration of 1.2M in GBL and DMSO (3:7). After solvation, the solution was filtered with a 200 nm PTFE filter and spin-coated on top of the relevant substrate at 1000 rpm (10 s), 5000 rpm (30 s), 6000 rpm (20 s). Crucially, 800 µL of toluene antisolvent was drop-casted onto the spinning film after 25 s to aid crystallisation. The film was then annealed at 100 ^oC for 10 minutes. This antisolvent treatment resulted in a colour change from pale yellow to pale brown, while annealing resulted in a dark brown film.

p-i-n films were made by depositing this layer on top of mesoporous TiO_2 and coating with a 10 mg/mL HTL solution. The spin-coating rotation speed was varied to ensure all HTL layers were 30 ± 5 nm thick. n-i-p films were prepared by first depositing the HTL onto the glass at 0.25 wt% in chlorobenzene. Next, 0.05 wt% PFN in MeOH was spin-coated at 4000 rpm (45 s) to provide a thin interlayer that ensures decent wetting of the $MAPbI_3$ layer. ETL solutions were prepared in chlorobenzene at 23 mg/mL and stirred at 40 ^oC for 1 hour and filtered with a 200 nm PTFE filter before use. These solutions were spin-coated on top of $MAPbI_3$ film at 2000 rpm (30 s).

Fabrication of n-i-p perovskite solar cells

n-i-p perovskite solar cells were fabricated on indium-doped tin oxide (ITO) coated glass substrates that were sequentially cleaned in acetone, detergent, deionised water (x2), acetone, and isopropanol (using ultrasonics) for 10 minutes. The substrates were then dried with nitrogen and treated by oxygen plasma for 10 minutes.

Tin(IV) oxide (15 wt % in H_2O colloidal dispersion, Alfa Aesar) was diluted with deionised water to 2.5 wt % and spin-coated onto ITO at 3000 rpm for 40 s. The films were immediately annealed at 150 °C for 30 minutes in ambient conditions forming a 25 nm SnO_2 nanoparticle film. The SnO_2 films were then cooled and further treated by oxygen plasma for 10 minutes to enable sufficient wetting for the next steps. The films were then transferred to a nitrogen filled glovebox for perovskite deposition. For the hole transport materials, a 10 mg/mL solution of PTAA (M_W = 14,000) and P3HT (M_W = 24,480) in toluene were prepared by stirring in a nitrogen filled glovebox for 1 h at 65 ^oC. In the case of our reference n-i-p cell, PTAA was doped following our previous report.[75] Briefly, additives of 8 µL bis(trifluoromethane)sulfonimide lithium salt (Li-TFSI)/acetonitrile (170 mg mL^{-1}, TCI) and 4 µL of 4-tert-butylpyridine (tBP, TCI) were added to the 10 mg/mL PTAA solution. The solution was then spin-coated onto the perovskite films at 3000 rpm for 20 s. Finally, 100 nm of Au was thermally evaporated (0.2 Å/s) at a base pressure of 5×10^{-6} mbar.

All current-voltage (J-V) characteristics were measured using a Keithley 2400 source meter. The cells were illuminated by an AM 1.5 filtered xenon lamp (Oriel Instruments) at 1 sun intensity, which was calibrated using a Si reference photodiode. All devices were stored in a dark nitrogen filled glovebox prior to measurement and were measured in a nitrogen-filled chamber.

X-Ray Photoluminescence (XPS)

The XPS measurements were obtained in MultiLab 2000 with the X-ray source provided by monochromated Al K α X-ray photons (hv = 14.9 keV). The core level spectra were performed with pass energy of 20 eV and step size of 0.05 eV.

Steady-State Photoluminescence (ss-PL)

Steady-state photoluminescence spectroscopy was performed with a Horiba Jobin-Yvan Fluorolog-3 spectrofluorometer at an excitation of 510nm and a slit width of 5nm.

Time-Resolved Photoluminescence (TRPL)

Time resolved photoluminescence spectroscopy (TRPL) was undertaken with a Horiba Deltaflex modular fluorescence lifetime system that uses a PPD 900 detector. Excitation of the sample was achieved with a 635nm LED (Horiba N-635L) at a rate of 1MHz and intensity of 18pJ/pulse. The half-life of the excitation pulse was 100ps.

Microsecond Transient Absorption Spectroscopy (TAS)

Samples for microsecond transient absorption spectroscopy measurements were taken in a sealed quarts cuvette from the nitrogen-filled glovebox where they had been prepared and excited with a dye laser (Photon Technology International Inc. GL-301) with fluence 10µJcm-2. The dye laser was itself pumped by a N_2 laser (Photon Technology International Inc. GL-3300). The transient changes in the absorption of the sample were captured with a 100W tungsten lamp (Bentham IL 1) on an orthogonal optical axis to the excitation beam. The probe wavelength was adjusted by a monochromator and set to the maximum of the transient spectrum of the HTL hole polaron. This probing beam was detected by a silicon

photodiode (Hamatsu Photonics, S1722-01) before being filtered and amplified (Costronics Electronics) and finally interpreted by a digital oscilloscope (Tektronics DPO3012).

The number of photoexcited carriers, n was approximated as follows:

$$n = \frac{E\lambda}{hcd}(1 - R_{pump} - T_{pump})$$

Where E is the energy density of the pump pulse, λ is the pump wavelength, d is the perovskite film thickness (= 350 nm) and R_{pump} and T_{pump} are the reflectance and transmittance at the pump wavelength measured via UV-Vis absorption spectroscopy. Here, we assumed that each absorbed photon created one electron/hole pair.

Associated Content

Supporting Information

Extraction of interfacial energetics from the literature; DEKTAK measurements for HTL thickness; HTL spin-coating parameters; Raw steady-state photoluminescence spectra for $MAPbI_3$/HTL films; Normalised photoluminescence spectra for $MAPbI_3$/HTL films with front and back excitation; Comparison of PL decay dynamics of $MAPbI_3$ and $MAPbI_3$:3HT; C 1*s* XPS spectra for $MAPbI_3$/HTL films; Transient absorption spectra of $MAPbI_3$/HTL films; Transient absorption spectrum of a $MAPbI_3$ film; Visible absorption of a $MAPbI_3$ film; TAS traces as a function of excitation fluence for $MAPbI_3$/PTPD; ΔOD_{max} as a function of n for Al_2O_3/$MAPbI_3$/HTL films; J-V characteristics of an ITO/SnO_2/PTAA/Au device; Transient absorption spectra of $MAPbI_3$/ETL films.

Conflicts of Interest

There are no conflicts to declare.

Acknowledgements

R.J.E.W was supported by the EPSRC Centre for Doctoral Training in Advanced Characterisation of Materials (grant number EP/L015277/1). S.A.H acknowledges support from EPSRC (grant numbers EP/R020574/1, EP/R023581/1, and EP/P032591/1). T.M.C acknowledges support from EPSRC grant number EP/N026411/1)

References

(1) National Renewable Energy Labs. Best Research-Cell Efficiency Chart; https://www.nrel.gov/pv/cell-efficiency.html (accessed Jul 1, 2021).

(2) Gong, J.; Darling, S. B.; You, F. Perovskite Photovoltaics: Life-Cycle Assessment of Energy and Environmental Impacts. *Energy Environ. Sci.* **2015**, *8*, 1953.

(3) Meggiolaro, D.; Motti, S. G.; Mosconi, E.; Barker, A. J.; Ball, J.; Riccardo, A.; Deschler, F.; Petrozza, A.; De Angelis, F. Iodine Chemistry Determines the Defect Tolerance of Lead-Halide Perovskites. *Energy Environ. Sci.* **2018**, *11*, 702–713.

(4) Yang, Y.; Yang, M.; Moore, D. T.; Yan, Y.; Miller, E. M.; Zhu, K.; Beard, M. C. Top and Bottom Surfaces Limit Carrier Lifetime in Lead Iodide Perovskite Films. *Nat. Energy* **2017**, *2*, 16207.

(5) Stolterfoht, M.; Wolff, C. M.; Márquez, J. A.; Zhang, S.; Hages, C. J.; Rothhardt, D.; Albrecht, S.; Burn, P. L.; Meredith, P.; Unold, T.; et al. Visualization and Suppression of Interfacial Recombination for High-Efficiency Large-Area Pin Perovskite Solar Cells. *Nat. Energy* **2018**, *3*, 847–854.

(6) Wang, J.; Fu, W.; Jariwala, S.; Sinha, I.; Jen, A. K. Y.; Ginger, D. S. Reducing Surface Recombination Velocities at the Electrical Contacts Will Improve Perovskite Photovoltaics. *ACS Energy Lett.* **2019**, *4*, 222–227.

(7) Tvingstedt, K.; Malinkiewicz, O.; Baumann, A.; Deibel, C.; Snaith, H. J.; Dyakonov, V.; Bolink, H. J. Radiative Efficiency of Lead Iodide Based Perovskite Solar Cells. *Sci. Rep.* **2014**, *4*, 6071.

(8) Aziz, A.; Aristidou, N.; Bu, X.; Westbrook, R. J. E.; Haque, S. A.; Islam, M. S. Understanding the Enhanced Stability of Bromide Substitution in Lead Iodide Perovskites. *Chem. Mater.* **2019**, *32*, 400–409.

(9) He, J.; Fang, W. H.; Long, R.; Prezhdo, O. V. Why Oxygen Increases Carrier Lifetimes but Accelerates Degradation of CH3NH3PbI3 under Light Irradiation: Time-Domain Ab Initio Analysis. *J. Am. Chem. Soc.* **2020**, *142*, 14664–14673.

(10) Aristidou, N.; Sanchez-Molina, I.; Chotchuangchutchaval, T.; Brown, M.; Martinez, L.; Rath, T.; Haque, S. A. The Role of Oxygen in the Degradation of Methylammonium Lead Trihalide Perovskite Photoactive Layers. *Angew. Chemie - Int. Ed.* **2015**, *54*, 8208–8212.

(11) Aristidou, N.; Eames, C.; Islam, M. S.; Haque, S. A. Insights into the Increased Degradation Rate of CH3NH3PbI3 Solar Cells in Combined Water and O2 Environments. *J. Mater. Chem. A* **2017**, *5*, 25469–25475.

(12) Aristidou, N.; Eames, C.; Sanchez-molina, I.; Bu, X.; Kosco, J.; Islam, M. S.; Haque, S. A. Fast Oxygen Diffusion and Iodide Defects Mediate Oxygen-Induced Degradation of Perovskite Solar Cells. *Nat. Commun.* **2017**, *8*, 15218.

(13) Chen, B.; Rudd, P. N.; Yang, S.; Yuan, Y.; Huang, J. Imperfections and Their Passivation in Halide Perovskite Solar Cells. *Chem. Soc. Rev.* **2019**, *48*, 3842–3867.

(14) Noel, N. K.; Abate, A.; Stranks, S. D.; Parrott, E. S.; Burlakov, V. M.; Goriely, A.; Snaith, H. J. Enhanced Photoluminescence and Solar Cell Performance via Lewis Base Passivation of Organic-Inorganic Lead Halide Perovskites. *ACS Nano* **2014**, *8* (10), 9815–9821.

(15) Su, T.; Eickemeyer, F. T.; Hope, M. A.; Jahanbakhshi, F.; Mladenovic, M.; Li, J.; Zhou, Z.; Mishra, A.; Yum, J.; Ren, D.; et al. Crown Ether Modulation Enables over 23% Efficient Formamidinium-Based Perovskite Solar Cells. *J. Am. Chem. Soc.* **2020**, *142* (47), 19980.

(16) Yang, S.; Dai, J.; Yu, Z.; Shao, Y.; Zhou, Y.; Xiao, X.; Zeng, X. C.; Huang, J. Tailoring Passivation Molecular Structures for Extremely Small Open-Circuit Voltage Loss in Perovskite Solar Cells. *J. Am. Chem. Soc.* **2019**, *141*, 5781–5787.

(17) Zhao, Y.; Zhu, P.; Huang, S.; Tan, S.; Wang, M.; Wang, R.; Xue, J.; Han, T.; Lee, S.; Zhang, A.; et al. Molecular Interaction Regulates the Performance and Longevity of Defect Passivation for Metal Halide Perovskite Solar Cells. *J. Am. Chem. Soc.* **2020**, *142*, 20071.

(18) Xu, W.; Hu, Q.; Bai, S.; Bao, C.; Miao, Y.; Yuan, Z.; Borzda, T.; Barker, A. J.; Tyukalova, E.; Hu, Z.; et al. Rational Molecular Passivation for High-Performance Perovskite Light-Emitting Diodes. *Nat. Photonics* **2019**, *13*, 418–424.

(19) Jariwala, S.; Burke, S.; Dunfield, S.; Shallcross, R. C.; Taddei, M.; Wang, J.; Eperon, G. E.; Armstrong, N. R.; Berry, J. J.; Ginger, D. S. Reducing Surface Recombination Velocity of Methylammonium-Free Mixed-Cation Mixed-Halide Perovskites via Surface Passivation. *Chem. Mater.* **2021**. doi: 10.1021/acs.chemmater.1c00848

(20) Wang, R.; Xue, J.; Meng, L.; Lee, J.-W.; Zhao, I.; Sun, P.; Cai, L.; Huang, T.; Wang, Z.; Wang, Z.-K.; et al. Caffeine Improves the Performance and Thermal Stability of Perovskite Solar Cells Caffeine Improves the Performance and Thermal Stability of Perovskite Solar Cells. *Joule* **2019**, *3*, 1464–1477.

(21) Kim, H.; Lee, C.; Im, J.; Lee, K.; Moehl, T.; Marchioro, A.; Moon, S.; Humphry-baker, R.; Yum, J.; Moser, J. E.; et al. Lead Iodide Perovskite Sensitized All-Solid-State Submicron Thin Film Mesoscopic Solar Cell with Efficiency Exceeding 9%. *Sci. Rep.* **2012**, *2*, 591.

(22) Westbrook, R. J. E.; Sanchez-Molina, I.; Marin-Beloqui, J. M.; Bronstein, H.; Haque, S. A. Effect of Interfacial Energetics on Charge Transfer from Lead Halide Perovskite to Organic Hole Conductors. *J. Phys. Chem. C* **2018**, *122*, 1326–1332.

(23) Schloemer, T. H.; Christians, J. A.; Luther, J. M.; Sellinger, A. Doping Strategies for Small Molecule Organic Hole-Transport Materials: Impacts on Perovskite Solar Cell Performance and Stability. *Chem. Sci.* **2019**, *10*, 1904–1935.

(24) Zhang, F.; Yao, Z.; Guo, Y.; Li, Y.; Bergstrand, J.; Brett, C. J.; Cai, B.; Hajian, A.; Guo, Y.; Yang, X.; et al. Polymeric, Cost-Effective, Dopant-Free Hole Transport Materials for Efficient and Stable Perovskite Solar Cells. *J. Am. Chem. Soc.* **2019**, *141*, 19700–19707.

(25) Tian, W.; Li, L. Identifying the Optimum Thickness of Electron Transport Layers for Highly Efficient Perovskite Planar Solar Cells. *J. Mater. Chem. A* **2015**, *3* (32), 16445–16452.

(26) Shao, Y.; Xiao, Z.; Bi, C.; Yuan, Y.; Huang, J. Origin and Elimination of Photocurrent Hysteresis by Fullerene Passivation in CH3NH3PbI3 Planar Heterojunction Solar Cells. *Nat. Commun.* **2014**, *5*, 5784.

(27) Lin, Y.; Shen, L.; Dai, J.; Deng, Y.; Wu, Y.; Bai, Y.; Zheng, X.; Wang, J.; Fang, Y.; Wei, H.; et al. π-Conjugated Lewis Base: Efficient Trap-Passivation and Charge-Extraction for Hybrid Perovskite Solar Cells. *Adv. Mater.* **2017**, *29*, 1604545.

(28) Xu, Y.; Wang, M.; Lei, Y.; Ci, Z.; Jin, Z. Crystallization Kinetics in 2D Perovskite Solar Cells. *Adv. Energy Mater.* **2020**, *10*, 2002558.

(29) Yao, Z.; Zhang, F.; Guo, Y.; Wu, H.; He, L.; Liu, Z.; Cai, B.; Guo, Y.; Brett, C. J.; Li, Y.; et al. Conformational and Compositional Tuning of Phenanthrocarbazole-Based Dopant-Free Hole-Transport Polymers Boosting the Performance of Perovskite Solar Cells. *J. Am. Chem. Soc.* **2020**, *142*, 17681–17692.

(30) Mo, Y.; Gao, J. Polarization and Charge-Transfer Effects in Lewis Acid-Base Complexes. *J. Phys. Chem. A* **2001**, *105* (26), 6530–6536.

(31) Im, S. H.; Lim, C.; Chang, J. A.; Lee, Y. H.; Maiti, N.; Kim, H.; Seok, S. Il. Toward Interaction of Sensitizer and Functional Moieties in Hole-Transporting Materials for Efficient Semiconductor-Sensitized Solar Cells. *Nano Lett.* **2011**, *11*, 4789–4793.

(32) Bi, D.; Yang, L.; Boschloo, G.; Hagfeldt, A.; Johansson, E. M. J. Effect of Different Hole Transport Materials on Recombination in CH3NH3PbI3 Perovskite-Sensitized Mesoscopic Solar Cells. *J. Phys. Chem. Lett.* **2013**, *4*, 1532.

(33) Jung, E. H.; Joon, J. N.; Park, E. Y.; Moon, C. S.; Shin, T. J.; Yang, T.-Y.; Noh, J. H.; Seo, J. Efficient, Stable and Scalable Perovskite Solar Cells Using Poly(3-Hexylthiophene). *Nature* **2019**, *567*, 511–515.

(34) Pearson, A. J.; Eperon, G. E.; Hopkinson, P. E.; Habisreutinger, S. N.; Wang, J. T. W.; Snaith, H. J.; Greenham, N. C. Oxygen Degradation in Mesoporous Al2O3/CH3NH3PbI3-XClx Perovskite Solar Cells: Kinetics and Mechanisms. *Adv. Energy Mater.* **2016**, *6*, 1600014.

(35) Stolterfoht, M.; Caprioglio, P.; Wolff, C. M.; Marquez, J. A.; Nordmann, J.; Zhang, S.; Rothhardt, D.; Hormann, U.; Amir, Y.; Redinger, A.; et al. The Impact of Energy Alignment and Interfacial Recombination on the Internal and External Open-Circuit Voltage of Perovskite Solar Cells. *Energy Environ. Sci.* **2019**, *12*, 2778–2788.

(36) Jeon, N. J.; Noh, J. H.; Kim, Y. C.; Yang, W. S.; Ryu, S.; Seok, S. Il. Solvent Engineering for High-Performance Inorganic-Organic Hybrid Perovskite Solar Cells. *Nat. Mater.* **2014**, *13*, 897–903.

(37) You, J.; Guo, F.; Qiu, S.; He, W.; Wang, C.; Liu, X.; Xu, W.; Mai, Y. The Fabrication of Homogeneous Perovskite Films on Non-Wetting Interfaces Enabled by Physical Modification. *J. Energy Chem.* **2019**, *38*, 192–198.

(38) Nam, S.; Kim, H.; Shin, M.; Lee, H.; Kim, Y. Wide Band Gap Triarylamine Derivative Doped with Organosulfonic Acid and Its Application for Organic Light-Emitting Devices. *J. Org. Semicond.* **2013**, *1* (1), 22–29.

(39) Aue, D. H.; Bowers, M. T. Chapter 9 - Stabilities of Positive Ions from Equilibreum Gas-Phase Basicity Measurements. *Gas Pase Ion Chem.* **1979**, *2*, 1–51.

(40) Kim, J.; Godin, R.; Dimitrov, S. D.; Du, T.; Bryant, D.; Mclachlan, M. A.; Durrant, J. R. Excitation Density Dependent Photoluminescence Quenching and Charge Transfer Efficiencies in Hybrid Perovskite/Organic Semiconductor Bilayers. *Adv. Energy Mater.* **2018**, *8*, 1802474.

(41) Endres, J.; Kulbak, M.; Zhao, L.; Rand, B. P.; Cahen, D.; Hodes, G.; Kahn, A. Electronic Structure of the CsPbBr3/Polytriarylamine (PTAA). *J. Appl. Phys.* **2017**, *121*, 035304.

(42) Xu, X.; Ma, C.; Cheng, Y.; Xie, Y.; Yi, X.; Guatam, B.; Chen, S.; Li, H.-W.; Lee, C.-S.; So, F.; et al. Ultraviolet-Ozone Surface Modification for Non-Wetting Hole Transport Materials Based Inverted Planar Perovskite Solar Cells with Efficiency Exceeding 18%. *J. Power Sources* **2017**, *360*, 157–165.

(43) Liu, H.; Li, M.; Yang, J.; Hu, C.; Shang, J.; Zhai, H. In Situ Construction of Conjugated Polymer P3HT Coupled Hierarchical ZnO Composite with Z-Scheme Enhanced Visible-Light Photocatalytic Activity. *Mater. Res. Bull.* **2018**, *106*, 19–27.

(44) Chen, P.; Bai, Y.; Wang, S.; Lyu, M.; Yun, J.; Wang, L. In Situ Growth of 2D Perovskite Capping Layer for Stable and Efficient Perovskite Solar Cells. *Adv. Funct. Mater.* **2018**, *28*, 1706923.

(45) Paternò, G. M.; Robbiano, V.; Fraser, K. J.; Frost, C.; Sakai, V. G.; Cacialli, F. Neutron Radiation Tolerance of Two Benchmark Thiophene- Based Conjugated Polymers: The Importance of Crystallinity for Organic Avionics. *Sci. Rep.* **2017**, *7*, 41013.

(46) Schneider, J.; Bahnemann, D. Strong Transient Absorption of Trapped Holes in Anatase and Rutile TiO2 at High Laser Intensities. *J. Phys. Chem. C* **2018**, *122*, 13979–13985.

(47) Enengl, C.; Enengl, S.; Pluczyk, S.; Havlicek, M. Doping-Induced Absorption Bands in P3HT : Polarons and Bipolarons. *ChemPhysChem* **2016**, *17*, 3836–3844.

(48) Haque, S. A.; Park, T.; Holmes, A. B.; Durrant, J. R. Transient Optical Studies of Interfacial Energetic Disorder at Nanostructured Dye-Sensitised Inorganic/Organic Semiconductor Heterojunctions. *ChemPhysChem* **2003**, *4* (1), 89–93.

(49) Makuta, S.; Liu, M.; Endo, M.; Nishimura, H.; Wakamiya, A.; Tachibana, Y. Photo-Excited Intensity Dependant Electron and Hole Injections from Lead Iodide Perovskite to Nanocrystalline TiO2 and Spiro-OMeTAD. *Chem. Commun.* **2016**, *52*, 673–676.

(50) Wang, Z.; Lin, Q.; Chmiel, F. P.; Sakai, N.; Herz, L. M.; Snaith, H. J. Efficient Ambient-Air-Stable Solar Cells with 2D–3D Heterostructured Butylammonium-Caesium- Formamidinium Lead Halide Perovskites. *Nat. Energy* **2017**, *2*, 17135.

(51) Isakova, A.; Topham, P. D. Polymer Strategies in Perovskite Solar Cells. *Polym. Phys.* **2017**, *55*, 549–568.

(52) Yang, W. S.; Park, B.; Jung, E. H.; Jeon, N. J.; Kim, Y. C.; Lee, D. U.; Shin, S. S.; Seo, J.; Kim, E. K.; Noh, J. H.; et al. Iodide Management in Formamidinium-Lead-Halide – Based Perovskite Layers for Efficient Solar Cells. *Science.* **2017**, *356*, 1376–1379.

(53) Lamberti, F.; Cescon, E.; Meneghetti, M.; Franco, L.; Lamberti, F.; Gatti, T.; Cescon, E.; Sorrentino, R.; Rizzo, A.; Menna, E.; et al. Evidence of Spiro-OMeTAD De-Doping by Tert -Butylpyridine Additive in Hole- Transporting Layers for Perovskite Solar Cells. *Chem* **2019**, *5*, 1806–1817.

(54) Ke, W.; Fang, G.; Liu, Q.; Xiong, L.; Qin, P.; Tao, H.; Wang, J.; Lei, H.; Li, B.; Wan, J.; et al. Low-Temperature Solution-Processed Tin Oxide as an Alternative Electron Transporting Layer for Efficient Perovskite Solar Cells. *J. Am. Chem. Soc.* **2015**, *137*, 6730–6733.

(55) Kuik, M.; Koster, L. J. A.; Wetzelaer, G. A. H.; Blom, P. W. M. Trap-Assisted Recombination in Disordered Organic Semiconductors. *Phys. Rev. Lett.* **2011**, *107*, 256805.

(56) Sah, C.-T.; Noyce, R. N.; Shockley, W. Carrier Generation and Recombination in P-N Junctions and P-N Junction Characteristics. *Proc. IRE* **1956**, *45*, 1228.

(57) Shao, S.; Abdu-aguye, M.; Qiu, L.; Lai, L.; Liu, J.; Palstra, T. T. M.; Kooi, B. J.; Hummelen, C.; Loi, M. A. Elimination of the Light Soaking Effect and Performance Enhancement in Perovskite Solar Cells Using a Fullerene Derivative. *Energy Environ. Sci.* **2016**, *9*, 2444–2452.

(58) Zheng, X.; Hou, Y.; Bao, C.; Yin, J.; Yuan, F.; Huang, Z.; Song, K.; Liu, J.; Troughton, J.; Gasparini, N.; et al. Managing Grains and Interfaces via Ligand Anchoring Enables 22.3%-Efficiency Inverted Perovskite Solar Cells. *Nat. Energy* **2020**, *5*, 131–140.

(59) Bai, S.; Da, P.; Li, C.; Wang, Z.; Yuan, Z.; Fu, F.; Kawecki, M.; Liu, X.; Sakai, N.; Wang, J. T.; et al. Planar Perovskite Solar Cells with Long-Term Stability Using Ionic Liquid Additives. *Nature* **2019**, *571*, 245.

(60) Lee, J.; Kang, H.; Kim, G.; Back, H.; Kim, J.; Hong, S.; Park, B.; Lee, E.; Lee, K. Achieving Large-Area Planar Perovskite Solar Cells by Introducing an Interfacial Compatibilizer. *Adv. Mater.* **2017**, *29*, 1606363.

(61) Wang, Y.; Liao, Q.; Chen, J.; Huang, W.; Zhuang, X.; Tang, Y.; Li, B.; Yao, X.; Feng, X.; Zhang, X.; et al. Teaching an Old Anchoring Group New Tricks: Enabling Low-Cost, Eco-Friendly Hole-Transporting Materials for Efficient and Stable Perovskite Solar Cells. *J. Am. Chem. Soc.* **2020**, *142*, 16632–16643.

(62) Deng, L.; Xie, S.; Gao, F. Fullerene-Based Materials for Photovoltaic Applications: Toward Efficient, Hysteresis-Free, and Stable Perovskite Solar Cells. *Adv. Electron. Mater.* **2018**, *4*, 1700435.

(63) Liu, H. R.; Li, S. H.; Deng, L. L.; Wang, Z. Y.; Xing, Z.; Rong, X.; Tian, H. R.; Li, X.; Xie, S. Y.; Huang, R. Bin; et al. Pyridine-Functionalized Fullerene Electron Transport Layer for Efficient Planar Perovskite Solar Cells. *ACS Appl. Mater. Interfaces* **2019**, *11*, 23982–23989.

(64) Li, B.; Zhen, J.; Wan, Y.; Lei, X.; Liu, Q.; Liu, Y.; Jia, L.; Wu, X.; Zeng, H.; Zhang, W.; et al. Anchoring Fullerene onto Perovskite Film via Grafting Pyridine toward Enhanced Electron Transport in High-Efficiency Solar Cells. *ACS Appl. Mater. Interfaces* **2018**, *10*, 32471–32482.

(65) Ohkita, H.; Ito, S. Transient Absorption Spectroscopy of Polymer-Based Thin-Film Solar Cells. *Polymer* **2011**, *52*, 4397–4417.

(66) Wu, T.; Wang, Y.; Li, X.; Wu, Y.; Meng, X.; Cui, D.; Yang, X.; Han, L. Efficient Defect Passivation for Perovskite Solar Cells by Controlling the Electron Density Distribution of Donor-π-Acceptor Molecules. *Adv. Energy Mater.* **2019**, *9*, 1803766.

(67) Fu, C.; Orgiu, E.; Perepichka, D. F. Face-on: Vs. Edge-on: Tuning the Structure of Tetrathiafulvalene Monolayers with Solvent. *J. Mater. Chem. C* **2018**, *6*, 3787–3791.

(68) Xiao, M.; Joglekar, S.; Zhang, X.; Jasensky, J.; Ma, J.; Cui, Q.; Guo, L. J.; Chen, Z. Effect of Interfacial Molecular Orientation on Power Conversion Efficiency of Perovskite Solar Cells. *J. Am. Chem. Soc.* **2017**, *139*, 3378–3386.

(69) Heo, J. H.; Im, S. H.; Noh, J. H.; Mandal, T. N.; Lim, C.-S.; Chang, J. A.; Lee, Y. H.; Kim, H.; Sarkar, A.; Nazeeruddin, M. K.; et al. Efficient Inorganic-Organic Hybrid Heterojunction Solar Cells Containing Perovskite Compound and Polymeric Hole Conductors. *Nat Phot.* **2013**, *7* (6), 486–491.

(70) Jones, T. W.; Osherov, A.; Alsari, M.; Sponseller, M.; Duck, B. C.; Jung, Y. K.; Settens, C.; Niroui, F.; Brenes, R.; Stan, C. V.; et al. Lattice Strain Causes Non-Radiative Losses in Halide Perovskites. *Energy Environ. Sci.* **2019**, *12*, 596–606.

(71) Jariwala, S.; Sun, H.; Adhyaksa, G. W. P.; Lof, A.; Muscarella, L. A.; Ehrler, B.; Garnett, E. C.; Ginger, D. S. Local Crystal Misorientation Influences Non-Radiative Recombination in Halide Perovskites. *Joule* **2019**, *3*, 3048–3060.

(72) Wu, Z.; Jiang, M.; Liu, Z.; Jamshaid, A.; Ono, L. K.; Qi, Y. Highly Efficient Perovskite Solar Cells Enabled by Multiple Ligand Passivation. *Adv. Energy Mater.* **2020**, *10*, 1903696.

(73) Chen, J.; Kim, S. G.; Ren, X.; Jung, H. S.; Park, N. G. Effect of Bidentate and Tridentate Additives on the Photovoltaic Performance and Stability of Perovskite Solar Cells. *J. Mater. Chem. A* **2019**, *7*, 4977–4987.

(74) Kamarudin, M. A.; Hirotani, D.; Wang, Z.; Hamada, K.; Nishimura, K.; Shen, Q.; Toyoda, T.; Iikubo, S.; Minemoto, T.; Yoshino, K.; et al. Suppression of Charge Carrier Recombination in Lead-Free Tin Halide

Perovskite via Lewis Base Post-Treatment. *J. Phys. Chem. Lett.* **2019**, *10*, 5277–5283.

(75) Macdonald, T. J.; Batmunkh, M.; Lin, C.; Kim, J.; Tune, D. D.; Ambroz, F.; Li, X.; Xu, S.; Sol, C.; Papakonstantinou, I.; et al. Origin of Performance Enhancement in TiO2-Carbon Nanotube Composite Perovskite Solar Cells. *Small Methods* **2019**, *3*, 1900164.